Visualization of uncorrelated, tandem symmetry mismatches in the internal genome packaging apparatus of bacteriophage T7

Fei Guo[a,1], Zheng Liu[a,1], Frank Vago[a], Yue Ren[a], Weimin Wu[a,2], Elena T. Wright[b], Philip Serwer[b], and Wen Jiang[a,3]

[a]Markey Center for Structural Biology, Department of Biological Sciences, Purdue University, West Lafayette, IN 47907; and [b]Department of Biochemistry, University of Texas Health Science Center, San Antonio, TX 78229

Edited by F. William Studier, Brookhaven National Laboratory, Upton, NY, and approved March 8, 2013 (received for review September 7, 2012)

Motor-driven packaging of a dsDNA genome into a preformed protein capsid through a unique portal vertex is essential in the life cycle of a large number of dsDNA viruses. We have used single-particle electron cryomicroscopy to study the multilayer structure of the portal vertex of the bacteriophage T7 procapsid, the recipient of T7 DNA in packaging. A focused asymmetric reconstruction method was developed and applied to selectively resolve neighboring pairs of symmetry-mismatched layers of the portal vertex. However, structural features in all layers of the multilayer portal vertex could not be resolved simultaneously. Our results imply that layers with mismatched symmetries can join together in several different relative orientations, and that orientations at different interfaces assort independently to produce structural isomers, a process that we call combinatorial assembly isomerism. This isomerism explains rotational smearing in previously reported asymmetric reconstructions of the portal vertex of T7 and other bacteriophages. Combinatorial assembly isomerism may represent a new regime of structural biology in which globally varying structures assemble from a common set of components. Our reconstructions collectively validate previously proposed symmetries, compositions, and sequential order of T7 portal vertex layers, resolving in tandem the 5-fold gene product 10 (gp10) shell, 12-fold gp8 portal ring, and an internal core stack consisting of 12-fold gp14 adaptor ring, 8-fold bowl-shaped gp15, and 4-fold gp16 tip. We also found a small tilt of the core stack relative to the icosahedral fivefold axis and propose that this tilt assists DNA spooling without tangling during packaging.

DNA packaging | precession | single particle cryo-EM | 3-D reconstruction | symmetry relaxation

The tailed dsDNA bacteriophages and human dsDNA viruses, such as herpesviruses and adenoviruses, share many features of structural organization and life cycle. Viruses of these diverse families evolved from a common ancestor that existed before the divergence of prokaryotes, archaea, and eukaryotes, the three domains of life (1–3). Assisted by a scaffolding protein, these viruses assemble a procapsid with a symmetrical, usually icosahedral, outer shell. One of the shell's 12 fivefold vertices is replaced by a symmetry-mismatched 12-fold portal. The dsDNA genome is subsequently pumped into the capsid chamber through the portal channel, accompanied by exit of scaffolding proteins. The energy-dependent DNA packaging process is performed by a complex machinery involving multiple, stacked layers at the portal vertex. Functions of the layers include DNA binding/loading (small terminase), ATPase hydrolysis (large terminase), DNA channel (portal), and DNA condensation (internal proteins, sometimes in several layers). The detailed structural basis and functional mechanism of the DNA packaging process are under extensive investigation (4–6).

Structural analysis of phage portal vertex and associated proteins has impact beyond understanding viral assembly. Symmetry mismatches also occur in the capping and branching of actin filaments to control cell shapes (7), and the reciprocating conformational changes of the two barrels of GroEL (Ping-Pong mode) to fold protein substrates (8). Although the details of symmetric structures have been routinely visualized, the details of both asymmetry and symmetry mismatch have only recently become visualizable with the development of single-particle cryo-EM and associated asymmetric 3D reconstruction methods (9–20). Both the symmetry-mismatched, coaxial 12-fold portal ring and the 5-fold capsid of several bacteriophages (9–11, 13, 15–18) were resolved simultaneously in asymmetric reconstructions, i.e., reconstructions in which no symmetry was imposed. Inside some bacteriophages, which include T7 (19, 21, 22), P-SSP7 (11), and ε15 (17), a roughly cylindrical, multilayered structure (that we will call the core stack) is attached to the portal ring. Diverse functions have been suggested for the core stack in capsid assembly, DNA packaging, and DNA ejection (4, 19, 23). Molecular-dynamics simulations have shown that the T7 core stack has a significant effect on packaged DNA conformation via excluded volume (24). The core stack might also play an active role in organizing the entering DNA during packaging (19, 21, 25). Knowledge of the core stack structure is needed to investigate its possible roles.

Additional symmetry mismatches exist in the core stack. An eightfold core layer of gene product 15 (gp15) was proposed for T7 based on cryo-EM and image analysis of T7 procapsids (21). Three layers of different but simultaneously resolved symmetries, 12-fold gp14, 8-fold gp15, and 4-fold gp16, were proposed primarily based on rotational analysis of the T7 procapsid asymmetric reconstruction (19), taking account of previous biochemical and symmetry analysis (21, 22, 26). This reconstruction revealed the outline of the core stack, but rotational smearing obscured structural details of the core stack, not only in T7 (19) but also in asymmetric reconstructions of phage P-SSP7 (11) and ε15 (17) (sections through reconstructions of all three phages are reproduced in Fig. S1). In the present work, we address the challenge of resolving structural details at each layer of the portal vertex of the T7 procapsid.

To reconstruct the portal vertex layers of T7, we have developed a technique that we call focused asymmetric reconstruction (FAR). By focusing alignment on neighboring layers, FAR extends the standard asymmetric reconstruction (SAR) method to resolve locally unique, but globally variable, structures in the T7 portal vertex. FAR reconstructions demonstrate a combinatorial assembly isomerism derived from joining together of structural elements, each with mismatched symmetry, in any of several different

Author contributions: P.S. and W.J. designed research; F.G., Z.L., F.V., Y.R., W.W., E.T.W., and W.J. performed research; W.J. analyzed data; and F.G., P.S., and W.J. wrote the paper.

The authors declare no conflict of interest.

This article is a PNAS Direct Submission.

Data deposition: The eight cryo-EM reconstructions (Icos, SAR, and FAR-I to FAR-VI) have been deposited in the Electron Microscopy Data Bank, www.emdatabank.org (accession nos. EMD-5556 through EMD-5573).

[1]F.G. and Z.L. contributed equally to this work.

[2]Present address: Laboratory of Structural Biology, National Institute of Arthritis and Musculoskeletal and Skin Diseases, National Institutes of Health, Bethesda, MD 20892.

[3]To whom correspondence should be addressed. E-mail: jiang12@purdue.edu.

This article contains supporting information online at www.pnas.org/lookup/suppl/doi:10.1073/pnas.1215563110/-/DCSupplemental.

orientations. This uncorrelated angular positioning and its associated isomerism causes smearing of SAR reconstructions.

Results

Icosahedral Reconstruction. Purified capsid I (i.e., procapsid) particles were plunge-frozen in vitreous ice and imaged using cryo-EM (Fig. 1*A*). The capsid I particles had spherical shape and were about 500 Å in diameter. For some of the particles, a ring-like feature was seen centered in the circular outline of the capsid shell. This feature is attributed to the portal/core stack structure viewed along the portal axis (21).

Icosahedral 3D reconstruction revealed a T = 7 icosahedral shell with skewed hexamers (Fig. S2*B*), as shown before in the procapsid structures of T7 (19, 26) and other tailed dsDNA phages (10, 27). In the icosahedral reconstruction, all of the nonicosahedral features, including the scaffolding protein (gp9) inside the gp10 shell and the portal/core stack complex, are smeared. In the radial density distribution, broad, relatively weak densities in the 100- to 200-Å radius range (Fig. S2 *A* and *C*) are presumably from smeared gp9 scaffolding protein. The gp10 shell at ∼245-Å radius abuts the scaffolding protein. The electron density of the core stack is seen at ∼55 Å radius, i.e., around the center of the capsid (Fig. S2 *A* and *C*).

SAR. SAR (i.e., without imposing any symmetry) was then performed using a symmetry relaxation method by iteratively searching for the best one among the 60 views related by icosahedral symmetry (i.e., icos→c1 symmetry relax) that matches the model projection to the particle image (17, 18). Without any assumption of the shape or location of the asymmetric structural features (*SI Text S1*), a large, hollow, barrel-shaped stack emerged at one of the icosahedral vertices with its axis apparently aligned with the neighboring icosahedral fivefold shell axis (Fig. 1 and Figs. S3 and S4). SAR produced the same icosahedral gp10 shell structure seen in the icosahedral reconstruction. However, pentons of gp10 were at only 11 of the 12 fivefold vertices. No penton density was observed at the 12th vertex, which is at the base of the stack. The missing penton left an opening in the gp10 shell (Fig. 1*C*).

The barrel-like stack was attached to the inner surface of the gp10 shell by relatively thin, ring-like densities that contact the five gp10 hexons surrounding the open vertex (Fig. 1 *C* and *D*). The stack was about 175 Å in diameter and about 295 Å in length with its distal end reaching beyond the center of the capsid. The small featureless ring at ∼55-Å radius in the icosahedral reconstruction (Fig. S2*A*) is produced by icosahedral averaging of the stack. As distance from the capsid center increased (beyond z2), rotational smearing in the icosahedral reconstruction weakened the core stack densities to a level indistinguishable to that of the diffused scaffolding protein densities (Fig. S2 and Icos column in Fig. 2).

Closer examination of the different axis-perpendicular sections of the SAR-derived, barrel-shaped core stack revealed turbine-like densities with apparent eightfold symmetry in the middle sections (Fig. 1*B* and z2 in SAR column of Fig. 2 and Fig. S3*B*, and column 12 of Fig. S4). However, only apparently smeared densities without discernable symmetries were observed in other regions of the core stack (z1, z3, and z4 in the SAR column in Fig. 2). Because the SAR reconstruction is the average of many particles, the smeared densities indicate that particles have variable structures in these regions. However, the presence of two regions of well-resolved structure (fivefold shell and eightfold middle sections of the stack), linked by intermediate regions with smeared density, is puzzling.

The regions of smeared density in SAR differed from those of asymmetric reconstructions of portal vertex in ε15 and P-SSP7 phages, although the size, shape, and position of this barrel-like stack in the T7 procapsid were similar to those of the combined portal and the core stack in ε15 (17) and P-SSP7 (11) phages.

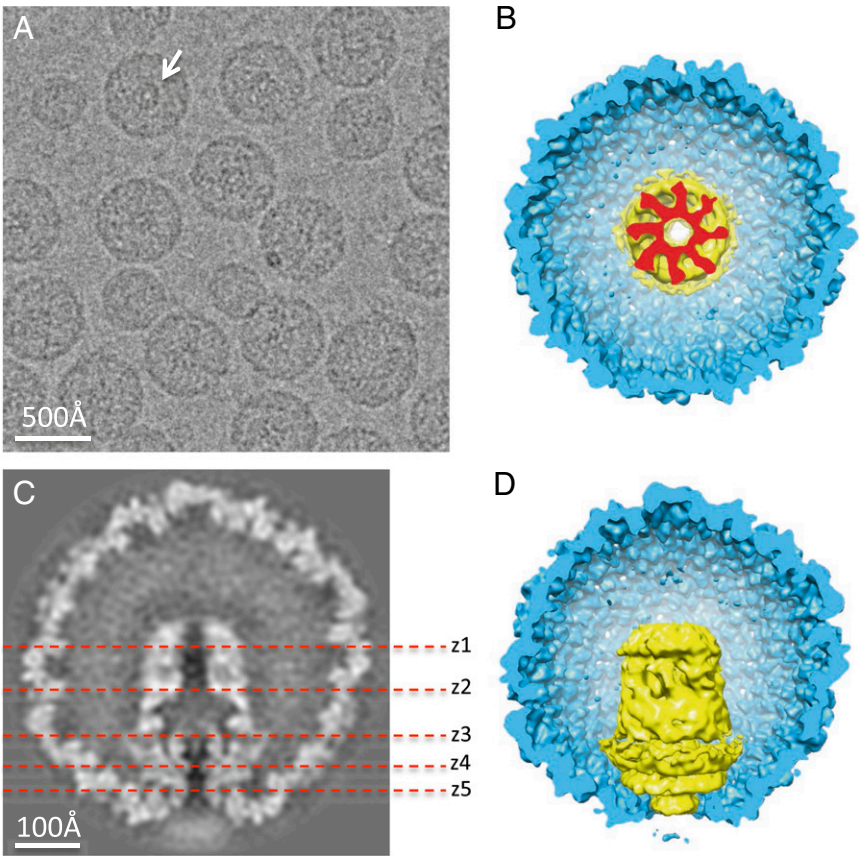

Fig. 1. SAR of T7 phage capsid I. (*A*) Cryo-EM image of particles embedded in vitreous ice. The arrow points to ring-like portal/core stack densities at the center of a capsid I particle viewed along the portal/core stack axis. The smaller round "particles" are contaminant vesicles. *B* and *D* display cut-open surface views parallel and perpendicular to the portal/core stack axis, respectively. *C* displays the density distribution in central section viewed perpendicular to portal/core stack axis (same view as in *D*). The dashed lines and corresponding labels (z1 to z5) indicate the sections displayed in subsequent figures (Fig. 2 and Figs. S3–S8). The images of these sections illustrate the symmetries of the core (gp16), core (gp15), core (gp14), portal (gp8), and shell (gp10) layers, respectively. The display in *B* was cut at section z2.

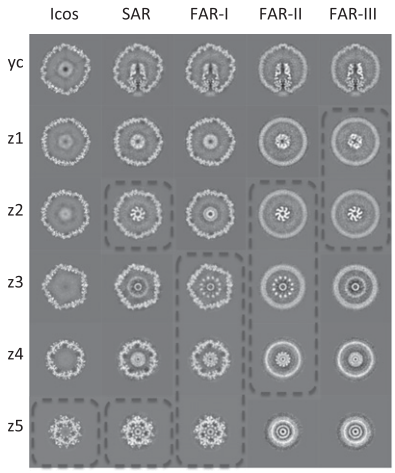

Fig. 2. FARs. Each column represents one of the labeled reconstructions (Icos, SAR, FAR-I, FAR-II, and FAR-III). The reconstructions are explained in the main text and also in Table S1. Row 1 (yc) shows the central sections of the five reconstructions cut parallel to the portal/core stack axis. The rest of the rows (z1, z2, z3, z4, z5) show different sections cut perpendicular to the portal/core stack axis at the position indicated by z number in Fig. 1C. The gray boxes indicate the sections with resolved densities in layers of the portal vertex.

Specifically, in the case of ε15 and P-SSP7, smearing was only seen at the distal end (i.e., the region closest to the capsid center), including the region corresponding to the eightfold region of T7 SAR reconstruction. The 12-fold portal was well resolved (Fig. S1). The z1 region was smeared for all three phages. These differences need to be explained with a more thorough understanding of the arrangement of the core stack, which is likely to include structural variability, as mentioned in the previous paragraph.

FARs. The SAR reconstructions of T7 capsid I (Fig. 1), ε15 (17), and P-SSP7 (11) phages implicitly assume that all particles have identical structure. When particles do not satisfy this assumption, the reconstruction, which is the average of all included particles, will only resolve those structural feature(s) (Fig. S1) that are the same among the particles and also dominant during the alignment. To overcome this limitation, we extended SAR by limiting the features used for alignment in both 3D reference map and 2D images. These features were limited to a region of interest, thereby excluding the contribution of other regions to the alignment. By varying the location and size of the included region, the alignment was targeted at feature(s) in the T7 procapsid that will be described below. We will refer this extension of SAR as FAR (see *SI Text S1* for more details).

We used the SAR reconstruction as starting model and limited the alignment to (*i*) the rotationally smeared portal and neighboring regions (i.e., sections around z3 to z5) and (*ii*) the neighboring region of the icosahedral shell (red circle in Fig. S5). This first FAR reconstruction (FAR-I) relaxed the fivefold cyclic symmetry to no symmetry (c5→c1 symmetry relax). In the resultant reconstruction (column FAR-I in Fig. 2 and Fig. S5), the icosahedral shell structure remained well resolved, as expected. However, the originally smeared portal region (i.e., sections around z3 to z5) in SAR now became well resolved with 12-fold symmetry, whereas the originally well-resolved eightfold core stack region (i.e., sections around z2) in SAR became rotationally smeared. The tip region (i.e., sections around z1) of the core stack remained smeared. FAR-I has revealed portal vertex layers in the order of 5-fold shell, 12-fold portal, and smeared region along the portal vertex axis. This is the same result obtained via SAR-like reconstructions for other phages (Fig. S1) (11, 17).

We then used FAR-I as starting model and focused the alignment on portal and entire core stack region (red circle in Fig. S6) to obtain FAR-II reconstruction (c12→c1 symmetry relax). FAR-II excluded the shell during alignment and produced a smeared shell, as expected. However, both the portal and part of the core stack (i.e., z2–z4 sections) were simultaneously well resolved as 12-fold and 8-fold symmetric structures, respectively (column FAR-II in Fig. 2 and Fig. S6). The tip region of the stack (z1) remained smeared. The SAR, FAR-I, and FAR-II reconstructions have collectively resolved details of any of the three binary combinations of the 5-fold shell, the 12-fold portal, and the 8-fold core. However, these details were not resolved simultaneously in any single reconstruction.

To resolve the core stack tip region (z1), another FAR reconstruction (c8→c1 symmetry relax) was performed (FAR-III column of Fig. 2; Fig. S7). In FAR-III, we included only sections around z1 and z2 in alignments (red circle in Fig. S7) and used the FAR-II reconstruction as initial model. In FAR-III, the region around section z2 of the core stack preserved its well-resolved eightfold densities, whereas the shell and portal region were both smeared. However, the tip region of the core stack now became clearly resolved, with fourfold symmetry (column FAR-III in Fig. 2).

To cross-validate these FARs from different routes of sequential asymmetric reconstructions, FAR-IV, FAR-V, and FAR-VI were performed (Fig. S8, with alignment regions listed). FAR-IV and FAR-V used SAR as starting model to sequentially resolve the 12-fold portal and the 5-fold shell, essentially in opposite direction to the sequential FAR-I/II reconstructions. Similar to FAR-I and FAR-II, binary combination of 8-fold core stack region and 12-fold portal region became resolved in FAR-IV, and binary combination of 12-fold portal region and 5-fold shell became resolved in FAR-V reconstruction. FAR-VI was performed similarly to FAR-III but used SAR as starting model. Binary combination of eightfold and fourfold core stack regions was also resolved in FAR-VI.

The eight reconstructions (Icos, SAR, and FAR-I to FAR-VI) are summarized in Table S1. The 5-fold shell, 12-fold portal, and 8-fold core stack were resolved in at least four different reconstructions. The fourfold core tip region was also resolved in two different reconstructions. Each of these structural components could be clearly resolved in asymmetric reconstructions from at least two different routes starting from SAR. These reconstructions have comprehensively examined and cross-validated the structural features in the portal vertex.

We produced a composite multilayer structure by including the resolved features extracted from these asymmetric reconstructions. Fig. 3 shows the composite structure, but this structure is only one of many assembly isomers for the following reason. Any two nearest-neighboring layers had a unique interface. However, no defined relative axial rotation existed between next-nearest neighboring and more distal layers. In other words, the multilayer portal vertex had numerous different structures instead of a single common one. That is the reason that neither SAR nor any single FAR could simultaneously resolve the entire portal vertex. We will call this arrangement of layers a stack with tandem uncorrelated symmetry mismatches. All isomers produced by the lack of correlation had a central channel that varied in diameter at different layers, but remained open throughout the entire assembly.

To our knowledge, this is the first time that tandem, uncorrelated symmetry mismatches have been visualized in a biological structure. In our case, four different rotational symmetries (5-, 12-, 8-, and 4-fold) are represented in the layers of the portal vertex. However, the basic concept is applicable to stacks with other symmetries and number of layers.

Structure and Composition of the Portal Vertex. The composite structure of Fig. 3 *A* and *B* was assembled from the individual components extracted from the FAR reconstructions (Fig. 3 *C*–*F*). Our assignment of structural features to the known capsid proteins is the same as that previously proposed (19, 21). The icosahedral shell was assigned to the only major capsid protein, gp10 (28). The 12-fold z5 region in FAR-I, FAR-II, FAR-IV, and FAR-V reconstructions was assigned to the portal protein, gp8, based on previous findings of both the same 12-fold

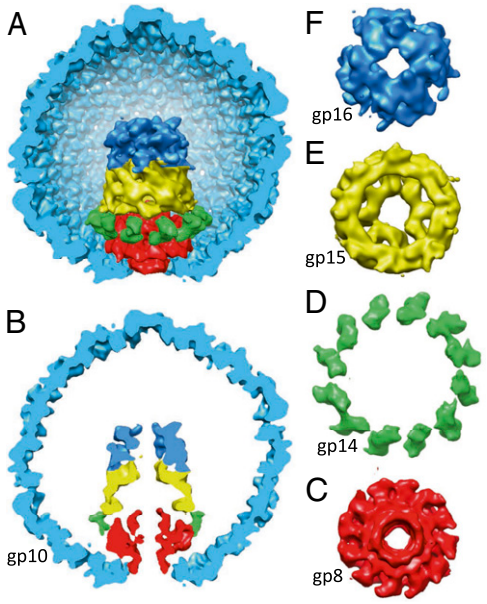

Fig. 3. Structure of the portal vertex. *A* and *B* each display a side view of a composite structure including the layers of the core stack (gp10 shell, gp8 portal, and gp14 core from FAR-I reconstruction, and gp15 and gp16 core from FAR-III reconstruction). *B* shows the 20-Å thick central slab. *C–F* display the axial view of 12-fold gp8, 12-fold gp14, 8-fold gp15, and 4-fold gp16, respectively. The composite structure is used here since none of the asymmetric reconstructions alone could resolve all five structural layers simultaneously. The composites in *A* and *B* represent only one of the numerous combinations of relative axial rotations of layer interfaces of portal vertex.

symmetry in the structures of both purified portal proteins and portal proteins attached to tails ejected from phage (29, 30).

The densities of the 12-fold gp8 layer superimpose well on the X-ray diffraction-derived, 12-fold atomic model of SPP1 (31) and P22 (32) phage portal rings (Fig. S9 *B–F*). However, the fitting of the cryo-EM structure of isolated T7 gp8 portal (30) was noticeably worse (Fig. S9*A*), which suggests assembly-dependent conformation for the T7 gp8 portal. The capsid I-associated T7 gp8 portal ring has three layers (Fig. S9*B*), with the middle layer (wing) much wider than the top (crown) and bottom layer (clip). The portal ring is mostly internal to the shell with only small contacts with the inner surface of the shell made by the tip of the clip layer (red region in Fig. 3; Fig. S9). The empty central channel of the portal ring varies in diameter with the narrowest region (~20 Å) formed by a ring of 12 projections equivalent to the tunnel loops in the SPP1 wing layer (Fig. S9*B*).

After subtracting the SPP1 portal structure from our reconstructions (FAR-I, FAR-II, FAR-IV, FAR-V), we were left with a 12-fold ring of densities around the z3 sections, which circumscribed the portal at the portal wing region. Because the SPP1 portal protein (502 aa) is similar in mass to T7 gp8 (536 aa), the extra densities were assigned to gp14 (196 a.a.), a core stack protein present in the capsid in an estimated 8–12 copies (Table S2) (21, 22). These 12-fold gp14 and gp8 densities were always coresolved or cosmeared in all eight reconstructions (Table S1). The gp14 protein appeared to be an adapter with relatively extensive contact with portal (gp8) and more tenuous contact with the eightfold layer of the core stack (Fig. 3).

The remaining core stack layers are an eightfold layer (around z2 sections in SAR, FAR-II, FAR-III, FAR-IV, and FAR-VI) and a fourfold layer (around z1 sections in FAR-III, FAR-VI) regions. Similarly, we confirm the previous assignments of these layers (19, 21), based on the estimated copy numbers and molecular masses of the known structural proteins (Table S2) (21, 22). The eightfold layer is assigned to gp15 and the fourfold layer is assigned to gp16 (Fig. 3).

The eightfold gp15 layer is an inverted, empty bowl with ~125-Å opening where it is loosely attached to the inner side of the 12-fold gp14 ring (Fig. 3, z2 to z3 sections in FAR-II and FAR-IV reconstruction). In contrast, the fourfold gp16 layer is more compact with a narrower channel (20-30 Å). The gp16 layer interacts extensively with the eightfold gp15 layer. The gp8, gp14, and gp15 layers collectively formed a large porous chamber (Fig. 3*B*) that is perhaps flexible and allows the core stack proteins to undergo conformational changes during procapsid assembly (22), DNA packaging (19), or DNA ejection at the beginning of an infection (23).

Symmetry Axis Offsets. Visually, the various layers of the portal vertex share a single axis in common with a fivefold axis of the icosahedral shell (Fig. 3 *A* and *B*). The resolutions of our reconstructions (Fig. S10) were sufficient to ask whether the axes of the various layers were indeed all aligned. We used the portal-associated fivefold shell axis as the reference (i.e., same as the icosahedral fivefold axis). Quantitative fitting of the symmetry axis of each layer (*SI Text S1*) revealed that, in fact, small offsets did exist (Fig. 4*A* and Fig. S11). The offset increased as the distance from the shell increased (Fig. 4*A*, Fig. S11, and Table S2). The 12-fold gp8 portal and gp14 rings are nearly coaxial with the reference 5-fold axis with insignificant offsets (<1 Å). However, an abrupt increase of offset to 4–5 Å occurred between the 12-fold gp14 ring and the 8-fold gp15 bowl (Fig. 4*A*). The offset further increased from 4 to 5 Å (gp15) to 7–8 Å (gp16) as distance from portal increased. The nearly linear increase of offsets from gp15 to

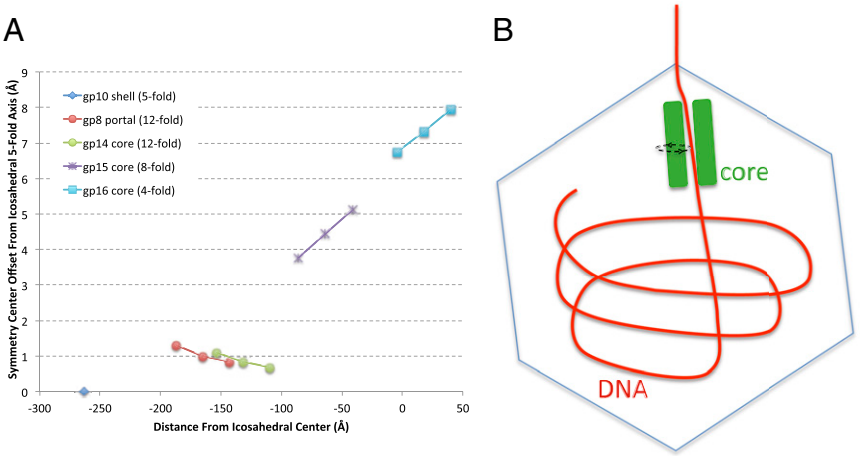

Fig. 4. Precession model of DNA packaging. (*A*) Center offsets for the symmetry axes of the structural layers in the portal vertex. The icosahedral fivefold axis is the reference. The symmetry axis position was separately determined for gp8, gp14, gp15, gp16 layers at three axial positions (mass center of each component and ±22 Å from mass center). (*B*) Schematic illustration of the proposed precession model for the packaged dsDNA emerging from distal opening of the central channel of the core stack. The slightly offset core stack precesses around the icosahedral fivefold axis and dispenses DNA in a circular pattern. When viewed from top to bottom in this illustration, the core stack will precess counterclockwise and the newly emerged DNA will form left-handed supercoil.

gp16 (Fig. 4*A*) suggests a slightly tilted (~1.6°) common axis for gp15 and gp16.

To determine whether the offsets were accumulative artifacts generated by the sequential FAR procedure, we have determined the core center offsets (Fig. S11*C*) for SAR, FAR-I, FAR-II, FAR-III, and previously reported capsid I structures (EMD-1161/1162) (19). Using the gp15 layer as representative, nearly identical center offsets were detected for FAR-II and FAR-III. In SAR, which is the starting model of FAR reconstructions, center offsets were also detected although at about one-half that of FAR-II and FAR-III. In contrast, only insignificant (<1 Å) center offsets were detected for the rest of the reconstructions (Fig. S11*C*). Thus, detectability of center offsets is strongly correlated with the rotational resolvability of core stack layer in the reconstructions.

Discussion

T7 Portal Vertex Layers Lack Long-Range Correlation in Their Axial Orientations. With our FARs, we have found that the T7 portal vertex varies in structure among different particles, even though each layer not only has unique structure, but also defined relationship to its nearest-neighboring layers, symmetry mismatched or not. This conclusion was drawn from the observations that (*i*) no single asymmetric reconstruction resolved all five layers stacked at the T7 portal vertex and (*ii*) at least one FAR resolved any two symmetry-mismatched, neighboring layers (summarized in Table S1). These observations imply that the axial orientations of distant layers (i.e., separated by one or more layers of different symmetry) are uncorrelated, which introduces the following constraint on assembly. The relative orientation of any layer has significant input only from the immediate neighboring layer but not from more distant layers. If, for example, the layers are assembled sequentially, then assembly information is not transferred through one layer to another.

Strictly speaking, in all cases of two layers separated by one or more intermediate layers of different symmetry, these two layers should not be simultaneously resolved. This prediction was found to be correct for the FAR reconstructions (FAR-I to FAR-VI, summarized in Table S1). Nonetheless, an exception was found in the SAR reconstruction that resolved fivefold gp10 and eightfold gp15 layers. These two layers were separated by the rotationally smeared 12-fold gp8/gp14 layer. Careful analysis of potential relative packing of layers with sequential 5-fold, 12-fold, and 8-fold symmetries (*SI Text S2* and Fig. S12) revealed that structural isomers with different choices of the intermediate 12-fold orientation had either exact or nearly exact alignment of the 8-fold layer to the 5-fold layer. Such alignment is exact for one-third of possible isomers or misaligned by angles of only 3° or less in the remaining two-thirds. Therefore, the SAR reconstruction is an average of heterogeneous mixture of structural isomers with properly resolved 5-fold and partially smeared 8-fold features sandwiching a highly smeared 12-fold layer.

To our knowledge, our resolving of the five layers of the T7 portal vertex is the first asymmetric reconstruction that has been achieved for any stack with uncorrelated and symmetry mismatched interfaces. The FAR procedures developed here are likely to be applicable to other stacks produced by combinatorial assembly isomerism.

A Paradigm in Structural Biology: Combinatorial Assembly Isomerism. SAR-like procedure, which was used for essentially all past asymmetric reconstructions (9–11, 13, 15–20), implicitly assumes that all particles included in a reconstruction have identical global structure and, therefore, that particle images differ only in the direction of the projection of this single structure (illustrated in Fig. S13*A*). For particles that all have the same component substructures, but have varying organization of the components among different particles (combinatorial assembly isomerism; illustrated in Fig. S13*B*), this assumption leads to reconstructions with only the dominant component(s) resolved, whereas the less dominant components are smeared. Examples include the asymmetric reconstructions of ε15 (17), P-SSP7 (11) (Fig. S1), and T7 SAR (Figs. 1 and 2, and Fig. S3). Combinatorial assembly isomerism is a relatively unexplored aspect of complex assemblies.

Our initial SAR reconstruction with smeared gp8 portal, but serendipitously resolved eightfold gp15 core stack layer, presented the paradox that motivated development of the FAR reconstruction strategy in this work. In the FAR reconstruction procedure, we explicitly consider the likelihood of combinatorial assembly isomerism. Each FAR selectively targets a contributing structural feature and minimizes the influence of other, possibly dominant structural features. By varying the region of focus, the various combinations of multiple stacked layers are resolved and cross-validated, as summarized in Table S1. That is to say, unlike SAR, the FAR reconstructions extend structural biology to a regime of structures with combinatorial assembly isomerism (*SI Text S3*).

Combinatorial assembly isomerism is a concept with well-known, analogous applications in the macroscopic world. An example is the assembling of different objects from a common set of LEGO pieces. The FAR reconstructions essentially deal with a special case of this regime in which the variations among stacked layers are constrained to discrete axial rotations, in analogy with what occurs in combination locks. Further method developments are needed to support determination of structures with combinatorial assembly isomerism that has more degrees of freedom.

T7 Core Stack Is Slightly Tilted from Its Icosahedral Fivefold Axis. A surprising finding of this study is that the T7 core stack, especially its gp15/gp16 layers, is slightly offset and tilted from the icosahedral fivefold axis of the portal vertex (Fig. 4*A* and Fig. S11). We found that all reconstructions with rotationally smeared core stack (SAR+C5, EMD-1161, EMD-1162, FAR-I, and FAR-III+C5) have an insignificant amount of center offset, whereas reconstructions with clearly resolved core stack (SAR, FAR-II, and FAR-III) (Fig. S11*C*) do have significant center offsets. This clear pattern indicates that the core stack does have a small offset and tilt, but that the offset and tilt can only be detected when at least the gp15 layer of the core stack is truly resolved. Rotational smearing is presumably the cause of the loss of the tilt and center offset in the other reconstructions of the T7 core stack (Fig. S11*C*). The reduced offset of SAR is caused by the partial rotational smearing of the SAR reconstruction (*SI Text S2*).

Core-Stack Precession Model for DNA Packaging. The tilt and offsets for the core stack (gp15/gp16 layers) imply the following aspect of DNA packaging, assuming that T7 DNA is packaged through the central channel of the portal/core stack and that the DNA molecule then emerges out of the channel of the core stack at the distal opening of gp16. While in the channel of the core stack, the dsDNA, which is semirigid with persistence length of 400–500 Å (33), exerts asymmetrical force on the central channel wall, pushed by packaging power strokes. The DNA molecule then exits the core stack at an off-center position (Fig. 4*B*).

We suggest the following hypothesis for existence of the core stack tilt, assuming that this tilt (*i*) is the product of evolutionarily selection and (*ii*) is maintained after the expulsion of the gp9 scaffolding protein and capsid expansion during DNA packaging (26). The asymmetrical force on the core stack causes at least one of the interfaces of the portal vertex layers to slip (rotate), assisted by the relatively low energy barriers implied especially by the weak interactions of the gp14/gp15 interface and the numerous (8 × 12) equivalent relative orientations of this interface (34). Slipping at the gp14/gp15 interface is also suggested by the abrupt increase of axis offsets at this position (Fig. 4*A*).

If so, the resultant slipping between layers of an offset core stack can cause precession of the core stack around the portal axis as illustrated in Fig. S14. Every 15° rotation of eightfold gp15 layer will align its next vertex to next vertex of 12-fold gp14 layer (30° + 15° = 45°). Twelve such rotations of the gp15 layer will

complete a revolution of gp15 layer precession around the portal axis. However, the gp15 layer has only rotated 180° (12*15° = 180°) around its own axis. The rate of gp15 layer precession around the portal axis is thus two times of the rate of its self-rotation in this model. The direction of gp15 layer precession is opposite to that of its self-rotation. This precession model is analogous to mechanical precession (35). Precession of the gp15/gp16 "nozzle" will cause dispensing of the emerging dsDNA in a circular pattern (Fig. 4*B*). From the measured T7 DNA packaging rate (~28 kb/min) (36) and assuming that the DNA forms the largest circles sterically allowed by the shell chamber, we estimate that the rate of the proposed precession will be around one to two revolutions per second. If the precession is unidirectional, the handedness of the DNA double helix is likely to bias toward left-handed supercoiling (Fig. 4*B*) similarly to dsDNA wrapping around histone in nucleosomes (37). It is possible that opposite direction or alternating directions could be adopted by the precession.

The proposed precession is one means to generate the observed coaxially packed genome in fully packaged infectious phage particles (17, 25) and also to explain lower than expected knotting previously observed in DNA packaged inside phage particles (38). The possibility of core stack rotation to assist DNA spooling has been previously suggested, although not as a precession (21, 25, 26). The precession, if unidirectional, would produce less twist than would be produced by the previously proposed portal rotation that tracks the DNA double helix (34, 39). Portal rotation is now known not to occur (40, 41). Finally, the core stack precession could be a response to evolutionary selection against tangling of DNA as it was packaged. A potentially analogous precession occurs when rhythmic gymnasts swing long ribbons to form spirals that do not tangle.

Related observations have been made in other systems. Tilting was also observed for the inner body of bacteriophage phiKZ around which was spooled the packaged DNA (42, 43). The P22 phage portal is not accompanied by a core stack. However, the P22 portal does have a surprisingly long C-terminal helical barrel, connected to a major domain by a flexible loop (Fig. S9*C*) (32). In P22 DNA genome packaging, this C-terminal helical barrel could serve a dispensing role similar to the proposed T7 core stack role, with the ring of connecting loops providing the flexibility for the helical barrel to precess.

Methods

Details of sample preparation, electron cryomicroscopy, image processing, and 3D reconstruction (icosahedral reconstruction, SAR, and FARs), and structural analysis are given in *SI Text S1*.

ACKNOWLEDGMENTS. This work was supported National Institutes of Health Grants R01AI072035, S10RR023011, and R01GM24365, and The Welch Foundation Grant AQ-764. The cryo-EM images were taken in the Purdue Biological Electron Microscopy Facility, and the Purdue Rosen Center for Advanced Computing provided the computational resource for the 3D reconstructions.

1. Baker ML, Jiang W, Rixon FJ, Chiu W (2005) Common ancestry of herpesviruses and tailed DNA bacteriophages. *J Virol* 79(23):14967–14970.
2. Bamford DH, Grimes JM, Stuart DI (2005) What does structure tell us about virus evolution? *Curr Opin Struct Biol* 15(6):655–663.
3. Abrescia NG, Bamford DH, Grimes JM, Stuart DI (2012) Structure unifies the viral universe. *Annu Rev Biochem* 81:795–822.
4. Black LW, Thomas JA (2012) Condensed genome structure. *Adv Exp Med Biol* 726: 469–487.
5. Feiss M, Rao VB (2012) The bacteriophage DNA packaging machine. *Adv Exp Med Biol* 726:489–509.
6. Serwer P (2010) A hypothesis for bacteriophage DNA packaging motors. *Viruses* 2(9): 1821–1843.
7. Ydenberg CA, Smith BA, Breitsprecher D, Gelles J, Goode BL (2011) Cease-fire at the leading edge: New perspectives on actin filament branching, debranching, and cross-linking. *Cytoskeleton (Hoboken)* 68(11):596–602.
8. Clare DK, et al. (2012) ATP-triggered conformational changes delineate substrate-binding and -folding mechanics of the GroEL chaperonin. *Cell* 149(1):113–123.
9. Tang J, et al. (2011) Peering down the barrel of a bacteriophage portal: The genome packaging and release valve in p22. *Structure* 19(4):496–502.
10. Chen DH, et al. (2011) Structural basis for scaffolding-mediated assembly and maturation of a dsDNA virus. *Proc Natl Acad Sci USA* 108(4):1355–1360.
11. Liu X, et al. (2010) Structural changes in a marine podovirus associated with release of its genome into Prochlorococcus. *Nat Struct Mol Biol* 17(7):830–836.
12. Choi KH, et al. (2008) Insight into DNA and protein transport in double-stranded DNA viruses: The structure of bacteriophage N4. *J Mol Biol* 378(3):726–736.
13. Tang J, et al. (2008) DNA poised for release in bacteriophage phi29. *Structure* 16(6): 935–943.
14. Leiman PG, et al. (2007) The structures of bacteriophages K1E and K1-5 explain processive degradation of polysaccharide capsules and evolution of new host specificities. *J Mol Biol* 371(3):836–849.
15. Xiang Y, et al. (2006) Structural changes of bacteriophage phi29 upon DNA packaging and release. *EMBO J* 25(21):5229–5239.
16. Lander GC, et al. (2006) The structure of an infectious P22 virion shows the signal for headful DNA packaging. *Science* 312(5781):1791–1795.
17. Jiang W, et al. (2006) Structure of epsilon15 bacteriophage reveals genome organization and DNA packaging/injection apparatus. *Nature* 439(7076):612–616.
18. Chang J, Weigele P, King J, Chiu W, Jiang W (2006) Cryo-EM asymmetric reconstruction of bacteriophage P22 reveals organization of its DNA packaging and infecting machinery. *Structure* 14(6):1073–1082.
19. Agirrezabala X, et al. (2005) Maturation of phage T7 involves structural modification of both shell and inner core components. *EMBO J* 24(21):3820–3829.
20. Morais MC, et al. (2001) Cryoelectron-microscopy image reconstruction of symmetry mismatches in bacteriophage phi29. *J Struct Biol* 135(1):38–46.
21. Cerritelli ME, et al. (2003) A second symmetry mismatch at the portal vertex of bacteriophage T7: 8-fold symmetry in the procapsid core. *J Mol Biol* 327(1):1–6.
22. Serwer P (1976) Internal proteins of bacteriophage T7. *J Mol Biol* 107(3):271–291.
23. Chang CY, Kemp P, Molineux IJ (2010) Gp15 and gp16 cooperate in translocating bacteriophage T7 DNA into the infected cell. *Virology* 398(2):176–186.
24. Petrov AS, Lim-Hing K, Harvey SC (2007) Packaging of DNA by bacteriophage epsilon15: Structure, forces, and thermodynamics. *Structure* 15(7):807–812.
25. Cerritelli ME, et al. (1997) Encapsidated conformation of bacteriophage T7 DNA. *Cell* 91(2):271–280.
26. Cerritelli ME, Conway JF, Cheng N, Trus BL, Steven AC (2003) Molecular mechanisms in bacteriophage T7 procapsid assembly, maturation, and DNA containment. *Adv Protein Chem* 64:301–323.
27. Gertsman I, et al. (2009) An unexpected twist in viral capsid maturation. *Nature* 458(7238):646–650.
28. Dunn JJ, Studier FW (1983) Complete nucleotide sequence of bacteriophage T7 DNA and the locations of T7 genetic elements. *J Mol Biol* 166(4):477–535.
29. Lander GC, et al. (2009) The P22 tail machine at subnanometer resolution reveals the architecture of an infection conduit. *Structure* 17(6):789–799.
30. Agirrezabala X, et al. (2005) Structure of the connector of bacteriophage T7 at 8A resolution: Structural homologies of a basic component of a DNA translocating machinery. *J Mol Biol* 347(5):895–902.
31. Lebedev AA, et al. (2007) Structural framework for DNA translocation via the viral portal protein. *EMBO J* 26(7):1984–1994.
32. Olia AS, Prevelige PE, Jr., Johnson JE, Cingolani G (2011) Three-dimensional structure of a viral genome-delivery portal vertex. *Nat Struct Mol Biol* 18(5):597–603.
33. Lu Y, Weers B, Stellwagen NC (2001-2002) DNA persistence length revisited. *Biopolymers* 61(4):261–275.
34. Hendrix RW (1978) Symmetry mismatch and DNA packaging in large bacteriophages. *Proc Natl Acad Sci USA* 75(10):4779–4783.
35. Wikipedia (2012) *Precession (Mechanical).* Available at http://en.wikipedia.org/wiki/Precession_(mechanical). Accessed December 23, 2012.
36. Son M, Watson RH, Serwer P (1993) The direction and rate of bacteriophage T7 DNA packaging in vitro. *Virology* 196(1):282–289.
37. Luger K, Mäder AW, Richmond RK, Sargent DF, Richmond TJ (1997) Crystal structure of the nucleosome core particle at 2.8 A resolution. *Nature* 389(6648):251–260.
38. Arsuaga J, et al. (2005) DNA knots reveal a chiral organization of DNA in phage capsids. *Proc Natl Acad Sci USA* 102(26):9165–9169.
39. Simpson AA, et al. (2000) Structure of the bacteriophage phi29 DNA packaging motor. *Nature* 408(6813):745–750.
40. Hugel T, et al. (2007) Experimental test of connector rotation during DNA packaging into bacteriophage phi29 capsids. *PLoS Biol* 5(3):e59.
41. Baumann RG, Mullaney J, Black LW (2006) Portal fusion protein constraints on function in DNA packaging of bacteriophage T4. *Mol Microbiol* 61(1):16–32.
42. Fokine A, et al. (2007) Cryo-EM study of the Pseudomonas bacteriophage phiKZ. *Structure* 15(9):1099–1104.
43. Wu W, Thomas JA, Cheng N, Black LW, Steven AC (2012) Bubblegrams reveal the inner body of bacteriophage φKZ. *Science* 335(6065):182.